

Revealing the origin of the vertical hysteresis loop shifts in an exchange biased Co/YMnO₃ bilayer

J. Barzola-Quiquia[‡], A. Lessig, A. Ballestar, C. Zandalazini[§],
G. Bridoux^{||}, F. Bern and P. Esquinazi[¶]

Division of Superconductivity and Magnetism, Institute for Experimental Physics II,
University of Leipzig, D-04103 Leipzig, Germany

Abstract. We have investigated exchange bias effects in bilayers composed by the antiferromagnetic o-YMnO₃ and ferromagnetic Co thin film by means of SQUID magnetometry, magnetoresistance, anisotropic magnetoresistance and planar Hall effect. The magnetization and magnetotransport properties show pronounced asymmetries in the field and magnetization axes of the field hysteresis loops. Both exchange bias parameters, the exchange bias field $H_E(T)$ as well as the magnetization shift $M_E(T)$, vanish around the Néel temperature $T_N \simeq 45$ K. We show that the magnetization shift $M_E(T)$ is also measured by a shift in the anisotropic magnetoresistance and planar Hall resistance having those a similar temperature dependence as the one obtained from magnetization measurements. Because the o-YMnO₃ film is highly insulating, our results demonstrate that the $M_E(T)$ shift originates at the interface within the ferromagnetic Co layer. To show that the main results obtained are general and not because of some special characteristics of the o-YMO₃ layer, similar measurements were done in Co/CoO micro-wires. The transport and magnetization characterization of the micro-wires supports the main conclusion that these effects are related to the response of the ferromagnetic Co layer at the interface.

PACS numbers: 75.60.-d,75.70.Cn

Submitted to: *JPCM*

[‡] E-mail: j.barzola@physik.uni-leipzig.de

[§] Present address: FaMAF-CLCM at University of Cordoba, Medina Allende S/N, 5000 Cordoba, Argentina.

^{||} Present address: Institut Catala de Nanotecnologia (ICN), Universitat Autònoma de Barcelona, E-08193 Bellaterra, Spain.

[¶] E-mail: esquin@physik.uni-leipzig.de

1. Introduction

Exchange bias effects are observed when a ferromagnetic (FM) thin layer is in atomic contact with an antiferromagnetic (AFM) layer. These effects are therefore directly related to an exchange coupling at their interface. Experimentally, they are generally observed as a shift of the hysteresis loop on the field axis when the bilayer is cooled from a temperature T_0 below the Curie temperature T_C of the FM layer but above the respective Néel temperature (T_N) of the AFM layer, to a temperature $T_1 < T_N$ in the presence of an external magnetic field H_{FC} . While magnetometry studies of the exchange bias effect and its shift in the field axis $H_E(T)$ [1, 2, 3] have been deeply performed since its discovery by Meiklejohn and Bean [4] when they investigated Co particles surrounded by their native antiferromagnetic oxide, there are a few comparative studies that used magnetotransport properties to elucidate exchange bias phenomena [5, 6, 7, 8, 9, 10]. Specially rare are the studies using the Hall effect [11]. Recently, however, the measurement of the exchange bias effects using the planar Hall effect has received considerable interest because of the higher signal-to-noise ratio compared with the magnetoresistance or spin valve configuration [12, 13, 14], a feature that might be promising for technology applications. On the other hand, the study of metal/oxide interfaces is a very attracting field that is gaining more relevance in the condensed matter community [15].

In the present work, we have investigated the exchange bias effects in a novel bilayer composed by a polycrystalline ferromagnetic (FM) Co film and a low temperature antiferromagnetic (AFM) oxide, namely o-YMnO₃ film. A further aim of this work is to study the exchange bias effects using different properties namely, SQUID magnetometry, longitudinal magnetoresistance (MR), anisotropic magnetoresistance (AMR) and the planar Hall effect (PHE). Besides the usual field shift effect characterized by the exchange bias field $H_E(T)$, of particular interest was the study of the magnetization shift $M_E(T)$, an exchange bias effect much less study in the past probably because of the smaller signal amplitude and technical difficulties, although recent reports in special exchange bias systems [16, 17] already showed that its magnitude can be large. In this work we show that this magnetization shift $M_E(T)$ not only can be systematically found in all measured properties but it has a similar temperature dependence as $H_E(T)$. The observation of these effects does not only support the existence of exchange bias in this system and its influence in both hysteresis loop axes, but it also demonstrates clearly that the magnetization shift $M_E(T)$ is directly related to the pinning of magnetic entities (magnetic moments or domain walls) [18, 19] within the FM Co layer at the interface and not in the AFM layer, in agreement with magnetization measurements reported recently in La_{0.7}Sr_{0.3}MnO₃/o-YMnO₃ bilayers [16]. This main conclusion of this study was possible simply because the transport properties do detect only the FM film and not the AFM film due to its highly insulating state at the temperatures of the measurements.

Because the o-YMO₃ layer is not a common AFM but a so called diluted

antiferromagnet in external magnetic field (DAFF), as will become clear in section 3.2.1, we decided to characterize both exchange bias effects, i.e. in the field as well as in the magnetization axis, in the archetype of exchange bias effects, namely in Co/CoO micro-wires. Our transport as well as magnetization characterization of the exchange bias effects not only agree each other but supports the main conclusion we get from the studies on the Co/o-YMO₃ bilayers, namely that the observed effects originate within the ferromagnetic Co layer, certainly due to the influence of the AFM layer at the interface. This was possible to conclude because of the negligible conductance of the CoO layer in comparison with that of Co. In this case the magnetoresistance measurements probe the FM Co layer and therefore may also contribute to the understanding of the FM depth profile[20].

2. Experimental Details

We prepared bilayers of FM Co thin films (selected for its weak anisotropy and small coercivity) covering an AFM orthorhombic o-YMnO₃ (o-YMO) layer grown on (100) SrTiO₃ substrates of area 6×6 mm². For the depositions of the o-YMO layer a KrF excimer laser (wavelength 248 nm, pulse duration 25 ns) was used. The growth parameters used for o-YMO were 1.7 J/cm² with 5 Hz repetition rate, 800°C substrate temperature and 0.10 mbar oxygen pressure during preparation. The thickness of the o-YMO film for the bilayer discussed in this report was 350 nm. The Co films were prepared by thermal evaporation under high vacuum (pressure $P \simeq 10^{-6}$ mbar) using a high purity Co (99,95%) precursor material. For the magnetization measurements we used a superconducting quantum interferometer device (SQUID) from Quantum Design. The substrate containing the AFM o-YMO layer was covered completely with 35 nm Co thin film. For the magneto-transport measurements we used a mask with defined shape to be able to measure the longitudinal and Hall resistances, see inset in Fig.6(b). These measurements were carried out immediately after the Co deposition and contacting the corresponding electrodes in a chip carrier.

The epitaxial growth of the o-YMO phase was confirmed by X-ray diffraction. The electrical transport measurements of the bilayer (at the temperature of the measurements the electrical transport is due only to the Co film) were performed with a high resolution AC bridge (LR700 from Linear Research) in a commercial cryostat in the temperature range between 5 K and 300 K with magnetic fields up to 4 T. The resistance of the highly resistive o-YMO film was measured using a Keithley 6517A electrometer. During the measurements, the temperature stability was better than 10 mK. A commercial Hall sensor and a resistance thermometer attached close to the sample were used to measure the magnetic field and temperature. The exchange bias effects were studied with the SQUID and magneto-transport under similar experimental conditions. Namely, the sample was heated up to 100 K $> T_N$ and a selected field was applied parallel to the main area of the sample. Then the sample was cooled down under this field to the selected temperature of the measurements. After the temperature

was stabilized, the field was swept in opposite direction and turned back to the initial field. This process was repeated for each selected temperature. A systematic study of the influence of the amplitude of the field H_{FC} used to prepare the field cooled state showed that the effects of minor loops, as for example any dependence of the coercive field, are negligible at $\mu_0|H_{FC}| \geq 0.3$ T. As was shown already in Ref. [16] for other bilayer exchange bias systems, the observed exchange bias effects reported here cannot be attributed to minor loop effects.

Cobalt thin films ($\simeq 50 \pm 5$ nm thickness) were deposited by thermal PVD at a base pressure of 10^{-7} mbar on a commercial 5×5 mm² p-boron doped silicon (100) substrates, capped with a 150nm Si₃N₄ layer. The cobalt micro-wires were produced using electron beam lithography (EBL) in a FEI NanoLab XT 200 Dual Beam microscope with a Raith ELPHY Plus extension at 10KV acceleration voltage. For the lithography process a commercial positive-working PMMA (950K) spin-coated on the substrates with a thickness of about 400 nm was used. The samples were prepared in up to three lithography processes. First the structure for the electrical contacts was written, which was sputtered in Ar atmosphere with a 5-10nm Pt/15-25nm Au bilayer. The base pressure of the vacuum chamber was 10^{-6} mbar, while the working pressure of the Ar sputter gas was 10^{-3} mbar. After lift-off and a new resist cover, the structures for the Co nanowires were written. In this paper we present the results of two Co/CoO samples, a single micro-wire of dimension (length between voltage electrodes \times width) $8 \mu\text{m} \times 0.7 \mu\text{m}$, and an array of 8,500 micro-wires for the magnetization measurements (length $50 \mu\text{m}$, $1 \mu\text{m}$ width), with a spacing of $20 \mu\text{m}$ to avoid interaction. The surface of the deposited cobalt films was analyzed *ex situ* by AFM measurements. The crystallite size ranges from ~ 25 nm to 40 nm; the surface roughness is rather small with a peak to peak height variation smaller than 4 nm. The measurements of the samples were done after leaving them two months in normal atmosphere for the formation of a natural, 3 ± 1 nm thick oxide film at the Co free surface.

The temperature dependence of the resistivity showed a linear behavior as one expects for a metal. Below 50 K a quadratic temperature dependence dominates. The residual resistivity ratio $\Gamma = \rho(300\text{K})/\rho(4\text{K})$ is rather small ($\Gamma \approx 1.5$) indicating that the nanowires are highly disordered. From the residual resistivity $\rho(4\text{K}) \approx 16 \mu\Omega\text{cm}$ we calculated the mean free path $l_{eff} = 6 \text{ nm} \dots 8 \text{ nm}$ (using the simple Drude formula $l_{eff} = m_e v_F / n e^2 \rho$, with $m_e = 9.1 \times 10^{-31}$ kg, $v_F = 1.5 \times 10^8$ cm/s, $n = 0.5 \times 10^{23}$ cm⁻³), a factor of five smaller than the observed grain size. The temperature dependent resistivity $\rho(300\text{K}) - \rho(4\text{K}) \approx 7.5 \mu\Omega\text{cm}$ is quite close to the literature values [21] giving $10.3 \mu\Omega\text{cm}$ in c-direction and $5.5 \mu\Omega\text{cm}$ in the perpendicular plane resulting in $7.1 \mu\Omega\text{cm}$ for a polycrystalline sample as is our case. This and the consistency throughout all of our samples indicate the good quality of the deposited material.

3. Results and discussion

3.1. X-ray characterization

The manganite of yttrium (bulk) usually has a hexagonal structure [22] but under high pressure and temperature it is transformed in the metastable orthorhombic phase [23, 24]. This energetically unfavorable phase in standard conditions can be reached in thin films if it grows pseudomorphic with the substrate [25]; in this case it can present different crystal domain structures and lattice strains [26]. We have prepared stable orthorhombic phase of YMO (o-YMO) epitaxially grown thin films on oriented (100) SrTiO₃ (STO) substrates by pulsed laser deposition, as has been reported earlier [27]. The phase of our prepared YMO samples was confirmed by X-ray diffraction using Cu-K_α line, see Fig. 1. The preferential growth of the (00l) planes is evident and corresponds to the orthorhombic YMO phase [27, 28]. According to our experimental resolution our film is purely orthorhombic but the presence of grain boundaries or certain texture should not be discarded. From the position peaks in the 2θ -scan, the out-of-plane lattice parameter is $c = 7.38 \text{ \AA}$, in good agreement with literature data [27, 28]. The peaks corresponding to the STO substrate are also present, see Fig. 1.

3.2. SQUID Magnetometry

3.2.1. Single o-YMnO₃ layer According to literature [29, 30] the o-YMO phase is AFM with Néel temperature $T_N = 42 \pm 2 \text{ K}$. In Fig. 2 we show the magnetic moment of a o-YMO thin film measured on warming after zero-field cooling (ZFC) and field cooling (FC) with an applied field $\mu_0 H = 20 \text{ mT}$. From the ZFC state we recognize a typical antiferromagnetic behavior. If we define the characteristic Néel temperature where the ZFC magnetic moment shows a maximum we obtain $T_N = 43.5 \pm 0.5 \text{ K}$ from the data in Fig. 2. If we define T_N , however, at the onset of a significant difference in magnetic moment between the FC and ZFC states $T_N = 58 \pm 2 \text{ K}$, see inset (b) in Fig. 2. It is also known that AFM fluctuations of the order parameter are established above [31] the actual T_N , overestimating in this way the value extracted from SQUID measurements. Whether the lowest or the upper temperature is the one where the exchange bias effects vanish, it will depend on the used experimental method and its sensitivity.

The behavior observed in the FC state, see Fig. 2, as well as in previous studies of o-YMO thin films [16], resembles that of diluted antiferromagnets in external magnetic field (DAFF). This suggests us to consider the domain state model (DS) [32, 33, 34, 35, 36] to describe the physical behavior of o-YMO films. It is well known that DAFF develop a domain state when cooled below T_N (sometimes showing a spin-glasslike behavior [37]) that leads to a net magnetization which couples to the external field. The work in Ref. [33] has demonstrated the broad range of applicability of this model, being possible to use it not only for single crystalline AFM, but also for any deviation of the perfect crystalline structure of the AFM, such as punctual defects, grain or twin boundaries. In particular, it has been applied in the exchanged-bias Co/Co_{1-y}O

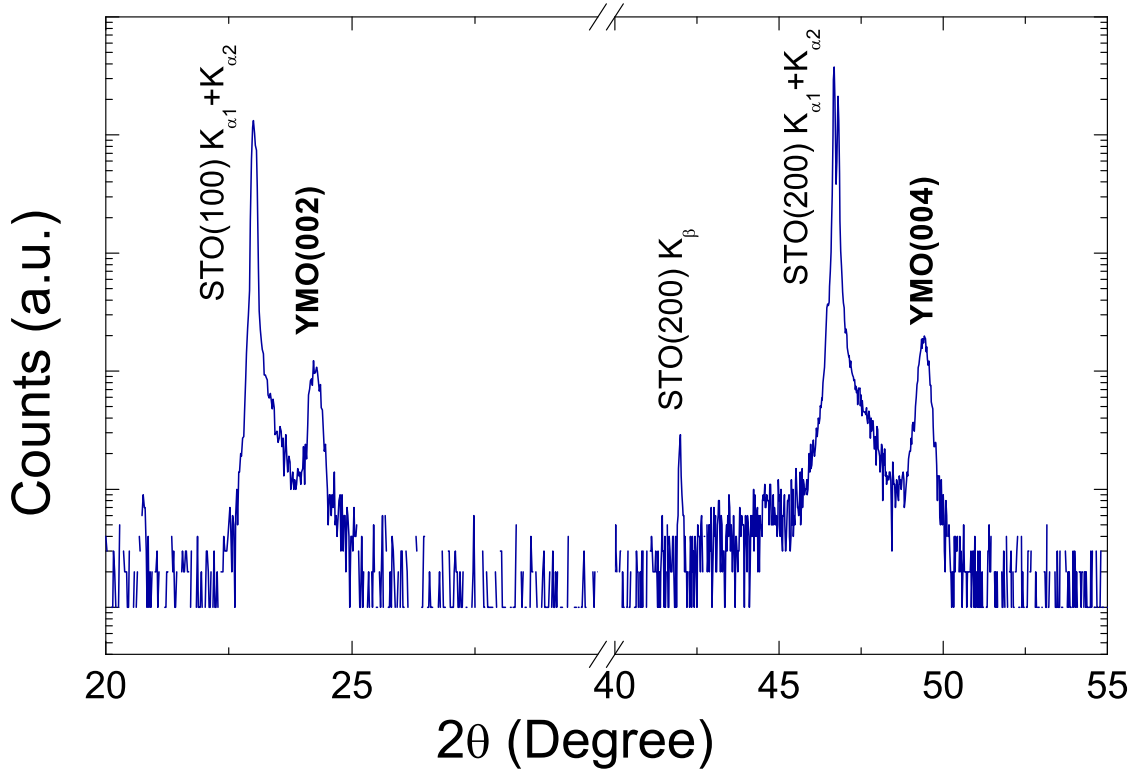


Figure 1. X-ray spectrum of the single o-YMO AFM layer deposited on a STO substrate used in our experiments. The thickness of the o-YMO film was 350 nm.

bilayer, where the Co_{1-y}O AFM layer presents crystallite sizes between 25 and 35 nm. Finally, it is important to note that the magnetic moment at saturation of our YMO film in the FC state is orders of magnitude smaller than that of the Co film. The inset (a) in Fig. 2 shows the hysteresis loop of the magnetization of the YMO single layer at 5 K, a loop characteristic of an AFM, being symmetric and without any vertical or horizontal shift. The magnetic moment at saturation and at 5 K is equal to 23 μemu . This means that the magnetic moment ratio at saturation between the FM and AFM layers for the bilayer sample is $\sim 10^2$. The tendency to saturation of $m(T \rightarrow 0)$ at a field of only 0.02 T shown in Fig. 2 is also typical for conventional DAFF materials.

Taking into account the results on the Co/CoO micro-wires we present below in section 4 we believe that a further discussion on whether our thin o-YMnO₃ layer behaves or not as a typical DAFF or whether this material is what we have at the interface with the layer Co, does not appear to us relevant, as will become clear after the presentation and discussion of the main results.

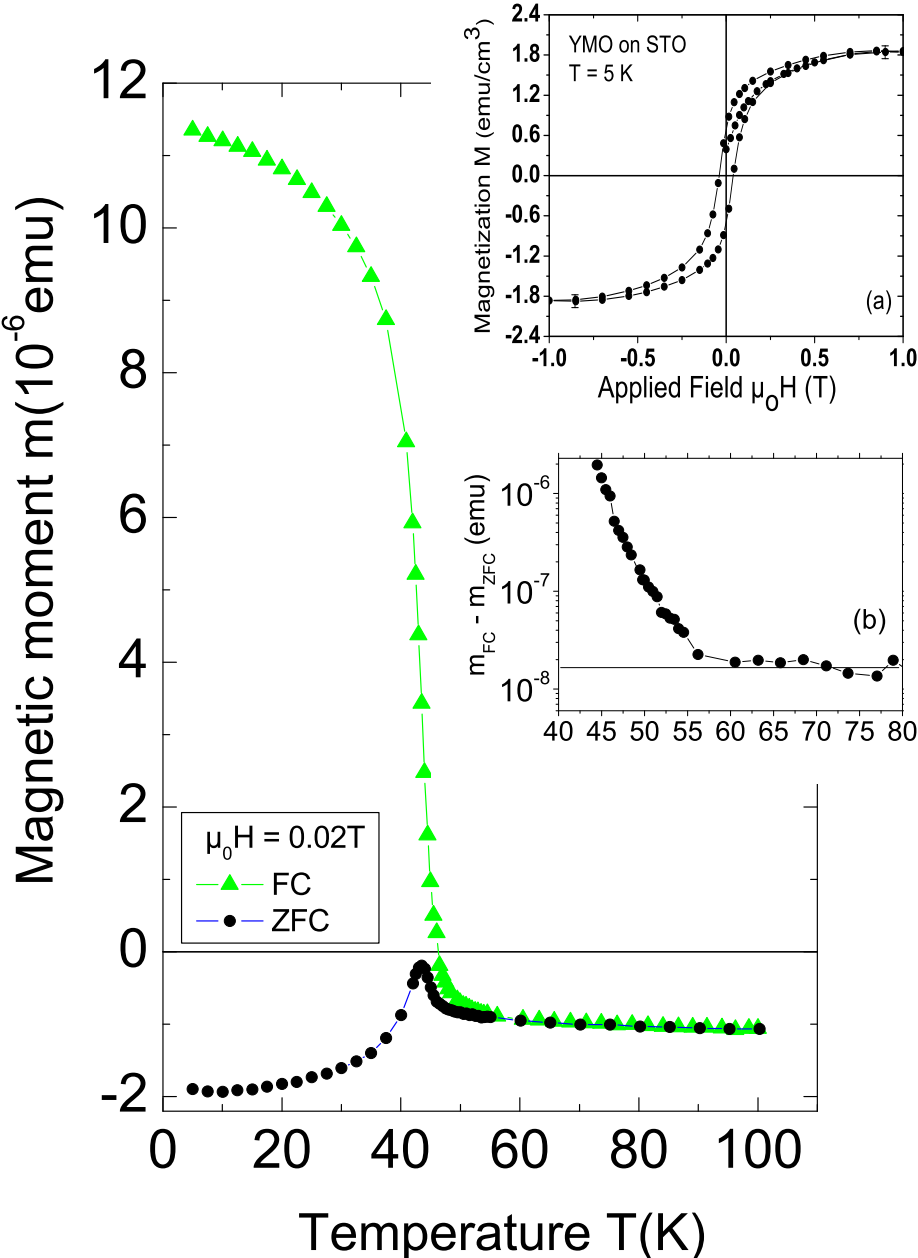


Figure 2. Magnetic moment vs. temperature of the o-YMO layer alone in the FC and ZFC states at a field of 20 mT. The field was applied parallel to the main area of the sample. In these results the diamagnetic contribution of the substrate was not subtracted. The inset (a) shows the field hysteresis of the magnetization at 5 K. The inset (b) below shows the difference between the two magnetic moment curves, at FC and ZFC states, of the main panel.

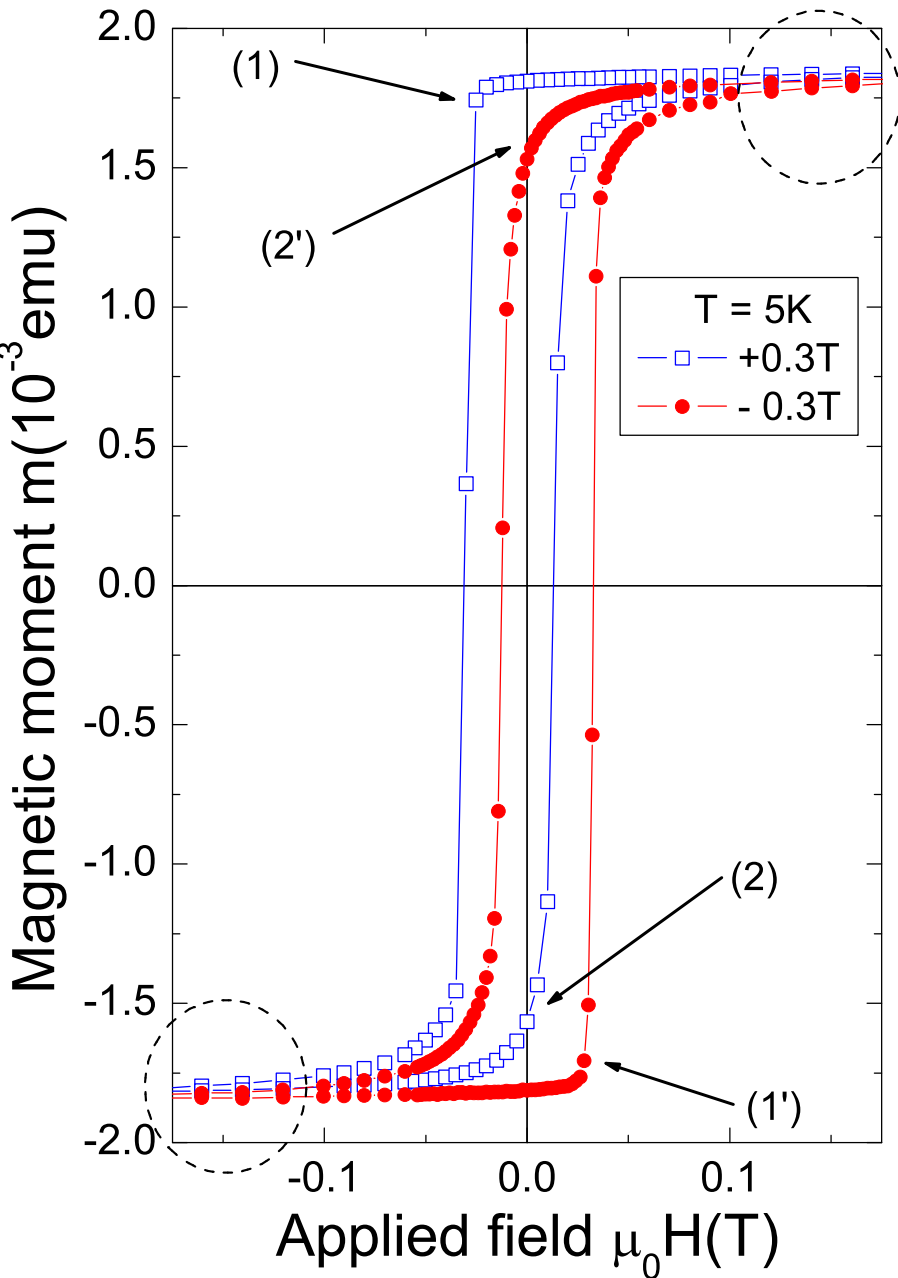


Figure 3. Hysteresis loops of the Co/o-YMO bilayer cooled to $T = 5\text{ K}$ at two fields $\mu_0 H_{FC} = \pm 0.3\text{ T}$. The two dashed circles indicate the regions where the vertical shift, the M_E effect, can be quantitatively characterized.

3.2.2. Bilayer Co/o-YMnO₃ It is well known that the exchange bias corresponds to an exchange field (H_E) transferred from the surface of the AFM into the FM, but its direction depends on the type of exchange coupling at the interface between the FM and AFM layers [36, 38]. Upon the magnetic characteristics of the layers material used (and in some cases also on the intensity of the applied field [39]) it is possible to found negative (usual case) as well as positive exchange bias [40] if the shift of the hysteresis loop along the field axis is in the opposite or same direction as the applied field, respectively. On the other hand, a vertical (magnetization) shift is observed if a number of frozen magnetic moments in one of the layers at the interface remains uncompensated due to the proximity to the other layer. Their orientation can be parallel or antiparallel with respect to the FM layer generating in this way a shift upwards of the hysteresis loops in case of a direct exchange or a shift downward in case of an indirect exchange mechanism [36, 41].

In order to corroborate the existence of the above described effects in our bilayer we have measured it by cooling with positive and negative magnetic fields ($H_{FC} = \pm 0.3$ T). The results obtained at $T = 5$ K are shown in Fig. 3. The shift in the magnetic field axis is clearly observed. We use the phenomenological definition for the strength of this effect characterized by the “exchange bias field” defined as $H_E = (H_C^+ + H_C^-)/2$, where H_C^+ and H_C^- are the coercive fields at positive and negative fields. In Fig. 3 we observe that the expected hysteresis shift depends on the sign of the H_{FC} . Within experimental resolution the absolute value of $|H_E(5\text{K})| \simeq 9$ mT is similar for both directions of H_{FC} .

The hysteresis loops show an asymmetry near the coercive fields where a change in the magnetization direction occurs. When the field is swept in the opposite direction as the one of H_{FC} , the magnetization remains constant up to the coercive field (positions (1) and (1') in Fig. 3) before a sudden change in the magnetic moment occurs. After reaching the saturation and reversing the field to the initial value, the magnetization curve remains nearly constant till the other coercive field is reached where the magnetic moment shows a rounded edge (arrows 2 and 2'). This asymmetric behavior in the magnetization is already known and it may have two different origins in an exchange bias system. One of them is related to a stable interface without training effect producing asymmetries explained in terms of a competition between magnetic field orientation, ferromagnetic and exchange-bias anisotropies [42]. The other one is intimately related to irreversible changes of the domain structure during the magnetization reversal, i.e. a training effect found in CoO/Co bilayers [43, 44, 45], for example. It is directly linked to a change in the magnetization reversal mechanism as a consequence of domain wall nucleation, domain wall propagation and rotation of the magnetization of the domains [35], i.e. an origin directly related to the ferromagnetic layer influenced by the interface. Although we do not present a direct study of training effects, the similarities of the observed asymmetries in the field loops in the magnetoresistance, a property directly related to the Co layer only, see Fig. 12(a), suggest that the observed asymmetry features have the same origin as in Co/CoO bilayers [43, 44, 45].

A detailed inspection of the data in Fig. 3 reveals a small but systematic shift in

the magnetic moment axis. This shift (at the regions within the dashed circles in Fig. 3) depends on the field direction used during the cooling process. In order to quantify the M_E effect we define the magnetic moment shift as $m_{\text{shift}} = (m_s^+ + m_s^-)/2$, where m_s^+ and m_s^- are the saturation moments at certain positive and negative fixed fields with the same absolute value. Our experimental setup for magnetic moment measurements uses a home developed sample holder [46], which allows a reproducibility and sensitivity of $\simeq 3 \times 10^{-7}$ emu at a field of 1 T. At the field of ± 0.3 T the reproducibility is of the order of 1×10^{-7} emu. From the data in Fig. 3 we obtain at $T = 5$ K a $m_{\text{shift}} = (9 \pm 0.5) \mu\text{emu}$ at $\mu_0 H_{FC} = 0.3$ T (see Fig. 5), nearly two orders of magnitude larger than our resolution and reproducibility limits. Note that this magnetic moment shift is huge, compared with the total magnetic moment at saturation of the AFM layer alone. In fact and taking the magnetization of the YMO layer alone, see inset (a) in Fig. 2, the total magnetic moment at saturation of the YMO layer is $23 \mu\text{emu}$. The observed $m_{\text{shift}} = 9 \mu\text{emu}$ would mean that about 135 nm YMO thick layer should contribute to the shift, a value obviously much larger than the expected exchange bias interface thickness. On the other hand magnetization loops of the YMO alone at different cooling fields H_{FC} show hysteresis loops without any vertical or horizontal shifts. Therefore, the origin of the M_E effect should not be in the YMO but in the Co layer at the interface, as the transport measurements also indicate.

The M_E effect in our bilayer can be interpreted as follows. After field cooling in an external field and due to the presence of the interfacial exchange field of the ferromagnetic layer, the AFM layer develops a frozen domain state that controls the exchange bias and the magnetic domains within the FM/AFM interface layer producing an irreversible surplus of magnetization at the FM side, as the experimental results indicate and in agreement with observations on $\text{La}_{0.7}\text{Sr}_{0.3}\text{MnO}_3/\text{o-YMnO}_3$ and $\text{La}_{0.67}\text{Ca}_{0.33}\text{MnO}_3/\text{o-YMnO}_3$ bilayers [16]. The formation and number of the domains within the FM Co layer that take part in the exchange bias coupling with the AFM layer can be enhanced leading to an increase of M_E . Therefore, the measured m_{shift} can be easily explained by pinned moments (or magnetic domains by domain wall pinning) within the FM layer at the interface, i.e. a pinned thickness of the order of 0.2 nm Co layer would be enough to produce the observed m_{shift} .

Figure 4 shows all the performed SQUID measurements at different temperatures when the sample was cooled with a positive H_{FC} . The exchange bias field H_E as well as the vertical shift m_{shift} in the magnetic moment obtained from the data in Fig. 4 are shown as a function of temperature in Fig. 5. These two quantities vanish between 45 K and 60 K, near the onset of the AFM transition, see Fig. 2, indicating that the measured effects should be a result of the exchange bias effect. At $T < 30$ K the exchange bias field follows $H_E(T) \propto (1 - T/T_N^*)$, where $T_N^* \simeq 32$ K is a kind of blocking temperature in general lower than the Néel temperature [1]. This linear dependence in T has also been observed in bilayer systems like FeO/Fe, CoO/Co and NiO/Ni [1] and theoretically predicted assuming a cubic anisotropy for the AFM material [47]. Note that the first sudden change in the magnetization (at (1) in Fig. 3) begins to be rounded

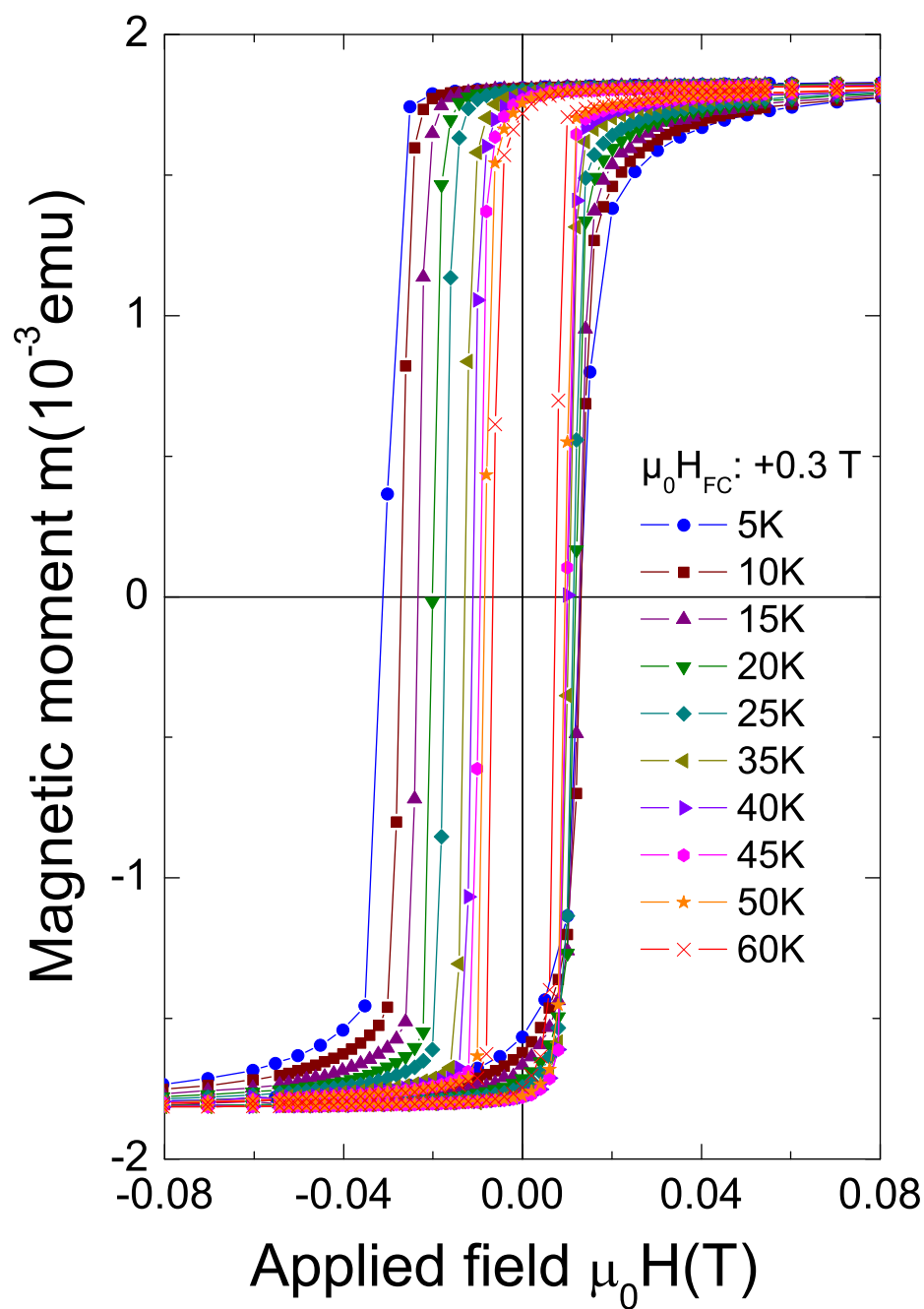


Figure 4. Hysteresis loops from SQUID measurements at different constant temperatures showing the exchange bias shift after cooling the sample with a positive magnetic field.

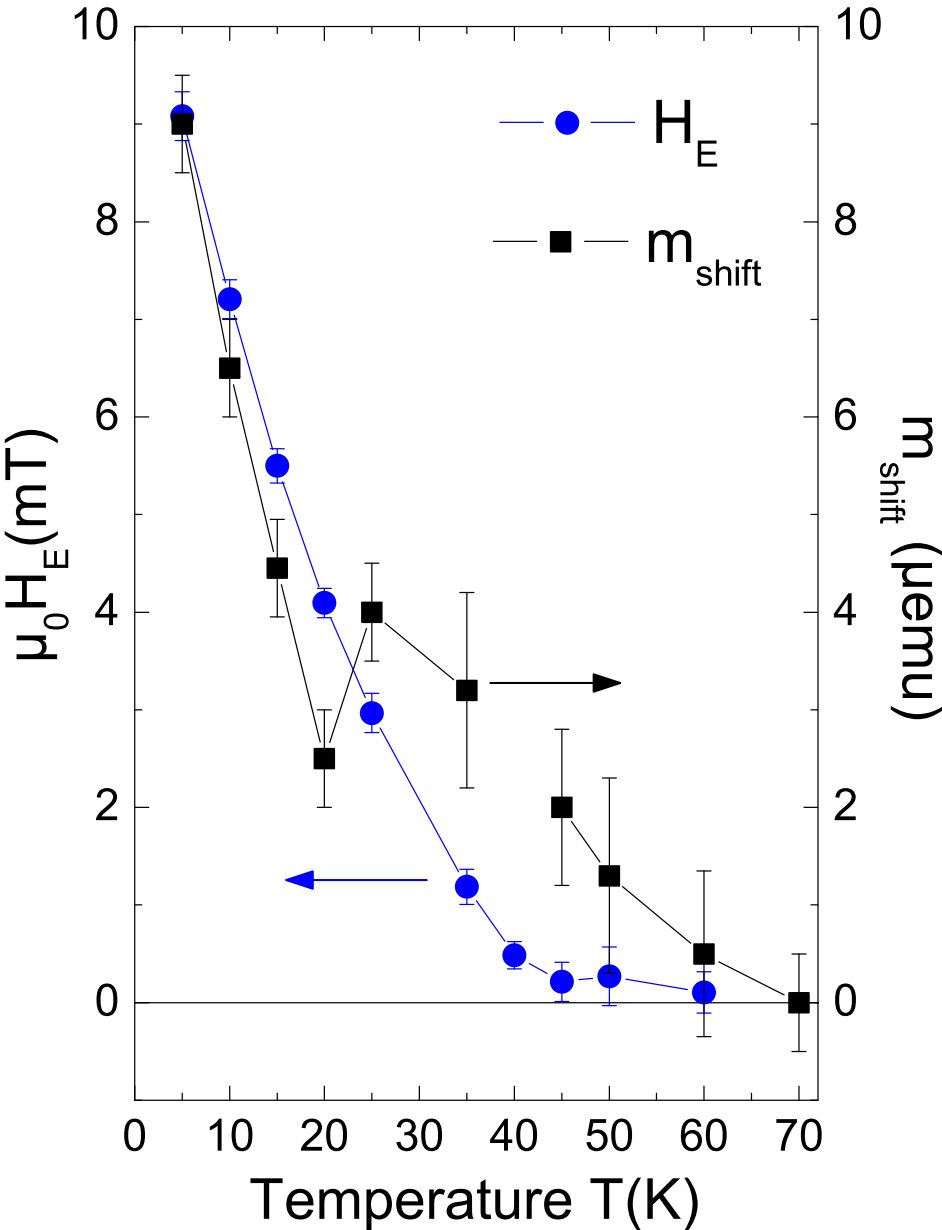


Figure 5. Temperature dependence of the exchange bias shift parameters obtained from the SQUID measurements after cooling the sample with a positive magnetic field of +0.3 T.

when the temperature approaches T_N , see Fig. 4, as a consequence of the weakening of the exchange coupling when the temperature increases. We note that both parameters $H_E(T)$ and $m_{\text{shift}}(T)$ show a similar – but not identical – temperature dependence, see Fig. 5. In particular there is a clear change of slopes at ~ 30 K and ~ 20 K in $m_{\text{shift}}(T)$, which is not observed in $H_E(T)$ within the resolution of the experiment. This anomaly in the temperature dependence is related very probably to the ferroelectric transition of o-YMO observed at $T \sim 30$ K [29, 30].

3.3. Magneto-transport measurements

In our bilayer the o-YMO layer deposited on STO serves as a dielectric substrate allowing us to measure the transport properties of the structured Co film deposited on the top. In order to warranty that the resistance contribution of the o-YMO layer is negligible compared to the Co layer, we have characterized similar YMO films using an electrometer with an upper resistance limit of $\sim 10^{10}$ Ω . The corresponding results are plotted in Fig. 6(a). The resistance of the o-YMO layer of similar thickness and area as the one used for the bilayer, shows a resistance of $\simeq 70$ M Ω at 290 K, in contrast to the resistance ~ 200 Ω of the Co layer, see Fig. 6(b). The increase in the resistance of the o-YMO layer decreasing temperature is huge and for $T < 160$ K the resistance is larger than the maximum we can measure. The resistance of the o-YMO film follows a variable range hopping (VRH) behavior given by the Efros-Shklovskii VRH dependence [48], as the inset in Fig. 6(a) indicates. The small deviation at low temperatures is an artifact due to the upper limit of the electrometer. Consequently, especially for temperatures $T < 100$ K the o-YMO layer behaves as an insulator in comparison to the resistance of the Co layer, giving us the possibility to explore the exchange-bias effects using magneto-transport properties that provide us direct information about the magnetic behavior of the FM layer and the influence of the exchange coupling of the AFM layer on it.

Figure 6(b) shows the temperature dependence of the resistance of the Co film deposited on the top of the o-YMO film. As expected, the observed behavior is typical for polycrystalline metallic Co in agreement with reported data [49]. The inset in this figure shows a sketch of the patterning of the Co sample used in this measurement and the magnetic field and electrical current directions.

Our experimental setup allows us to perform angular dependent measurements changing the angle α , see Fig. 6(b), from 0° to 270° . It is known that magneto-electrical transport measurements on conducting ferromagnets can provide information about their magnetic properties, as, e.g., the transition temperature, the easy axis direction, the coercivity, etc. We have measured the so called anisotropic magnetoresistance (AMR) and the planar Hall effect (PHE). The experimental conditions for such measurements are similar to the classical magnetoresistance (MR) and Hall effect, but the magnetic field \mathbf{H} is applied parallel to the sample main plane formed by x and y (see Fig. 6(b)). For this field direction the AMR is the resistance measured between electrode

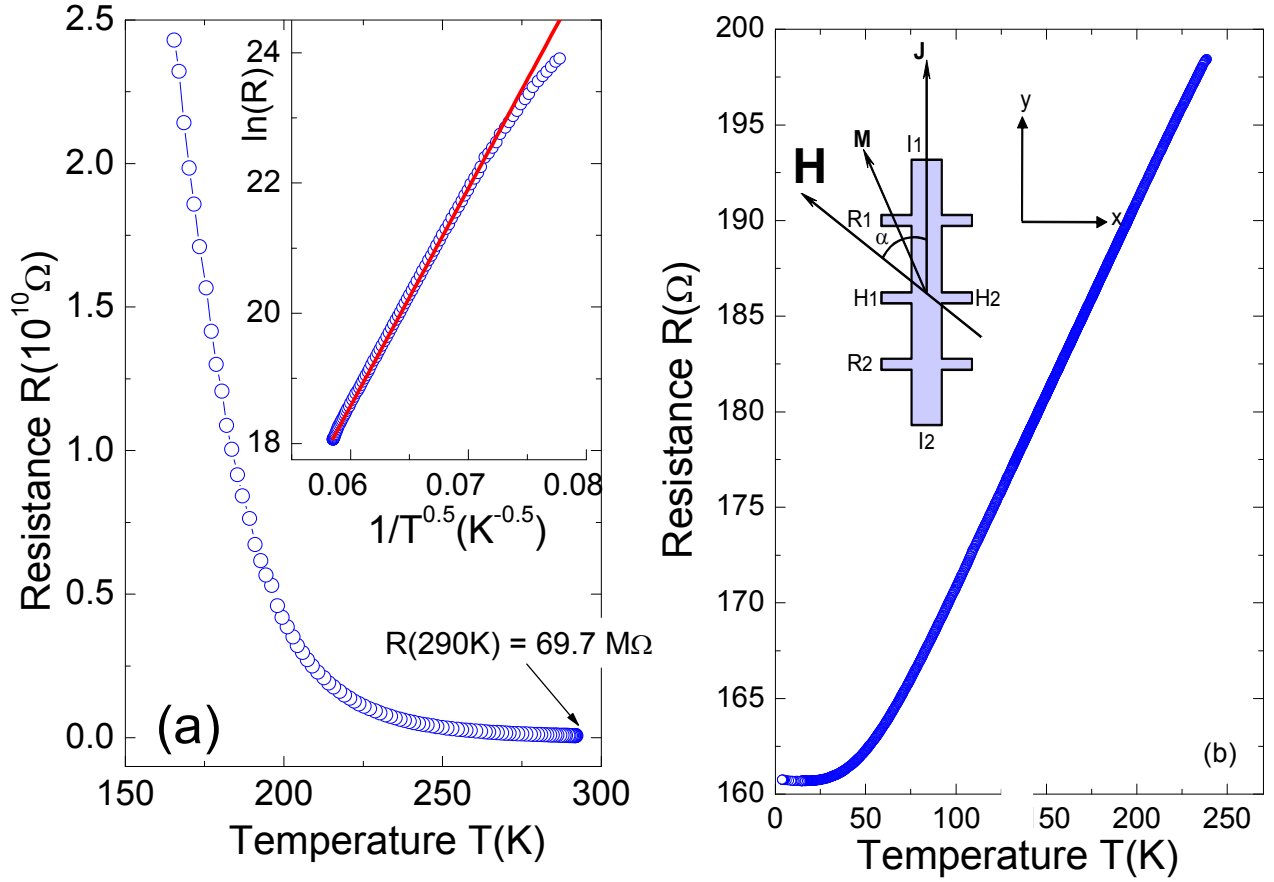


Figure 6. Temperature dependence of the resistance for (a) the YMO film alone, and (b) the Co film deposited on the top of the YMO. The inset in (a) shows the same data for the YMO layer but in a semilogarithmic scale vs. $T^{-0.5}$ and the inset in (b) shows the sample geometry and electrodes used for the measurements of the bilayer. The arrows show the field H applied at an angle α from the main (current) axis and an arbitrary magnetization direction M out of the main axis and on the sample main plain.

R_1 and R_2 of Fig. 6(b)), and the PHE is the voltage measured between electrodes H1 and H2 of Fig. 6(b). Assuming a single-domain model, the AMR as a function of the angle is given by

$$R_{AMR}(\alpha) = R_{\perp} + (R_{\perp} - R_{\parallel}) \cos^2 \alpha, \quad (1)$$

and the PHE is

$$R_{PHE}(\alpha) = (R_{\parallel} - R_{\perp}) \cos \alpha \sin \alpha, \quad (2)$$

where R_{\parallel} and R_{\perp} are the resistances when the magnetization is parallel and perpendicular to the current, respectively. The difference between R_{\parallel} and R_{\perp} is the origin for the anisotropic magnetoresistance and the planar Hall effect. Figure 7 shows the AMR and PHE at room temperature as a function of the angle α . The good fits using the above equations confirm the single-domain model assumption at the applied

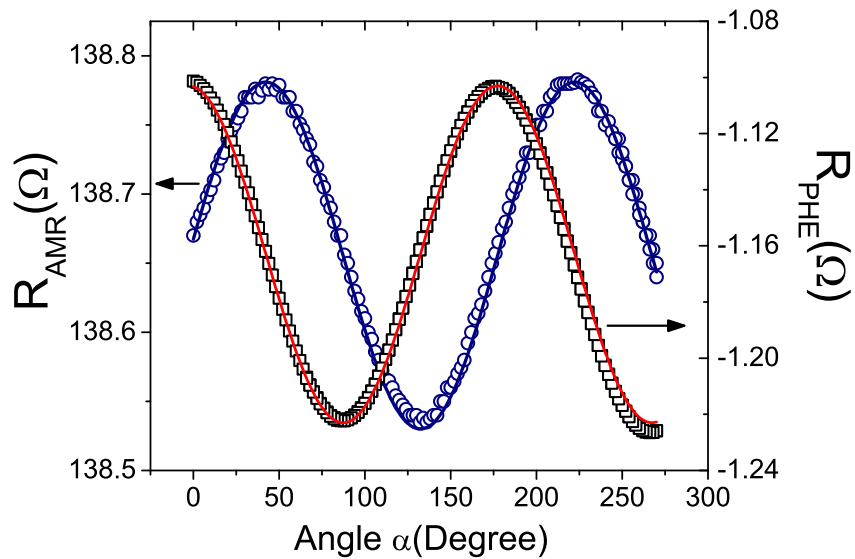


Figure 7. Anisotropic magnetoresistance (AMR) and planar Hall effect (PHE) measured at room temperature using a field of $\mu_0 H = +0.25$ T. Due to the alignment of the sample inside the sample holder at an angle $\alpha = 43^\circ$ the magnetic field is parallel to the main samples axis, i.e. parallel to the current direction. The continuous lines are the fits to Eqs. (1) and (2) with the same parameter $R_{\parallel} - R_{\perp} = 0.25 \Omega$ and $R_{\perp} = 138.53 \Omega$.

field. Due to the large value of R_{\perp} , one can realize that the relative change in the PHE is larger than the one of AMR, making the first one a more sensitive tool to study magnetic effects produced by the exchange bias.

We have performed the PHE measurements in a ZFC state at different constant temperatures, i.e. above and below T_N , and the angular dependent measurements cycling from $\alpha = 0^\circ$ to $\alpha = 270^\circ$ and back to $\alpha = 0^\circ$. At temperatures above 100 K the results follow Eq. (2), see Fig. 8, while below 100 K a hysteresis is observed although there is no difference between the initial and final R_{PHE} values within experimental resolution. This reversibility of the initial and final R_{PHE} values after cycling the field remains also at different applied fields as Fig. 9 shows. From these results we conclude that independently of the applied field, starting always from a ZFC state, there is no irreversibility between the initial and final values of the PHE after cycling the angle. The hysteresis observed at angles $\alpha \neq 0^\circ$ is a natural consequence of the cobalt ferromagnetic hysteresis.

Figure 10 shows PHE measurements in the FC state where it becomes evident that after a cycle the PHE resistance at the end of the cycle is not the same, i.e. a clear PHE-shift appears at the end of the loop in clear contrast to the ZFC measurements. On the other hand, the hysteresis observed at angles $\alpha \neq 0^\circ$ in ZFC is also present in the FC state. Consequently, this hysteretic feature, the PHE-shift at the end of cycle,

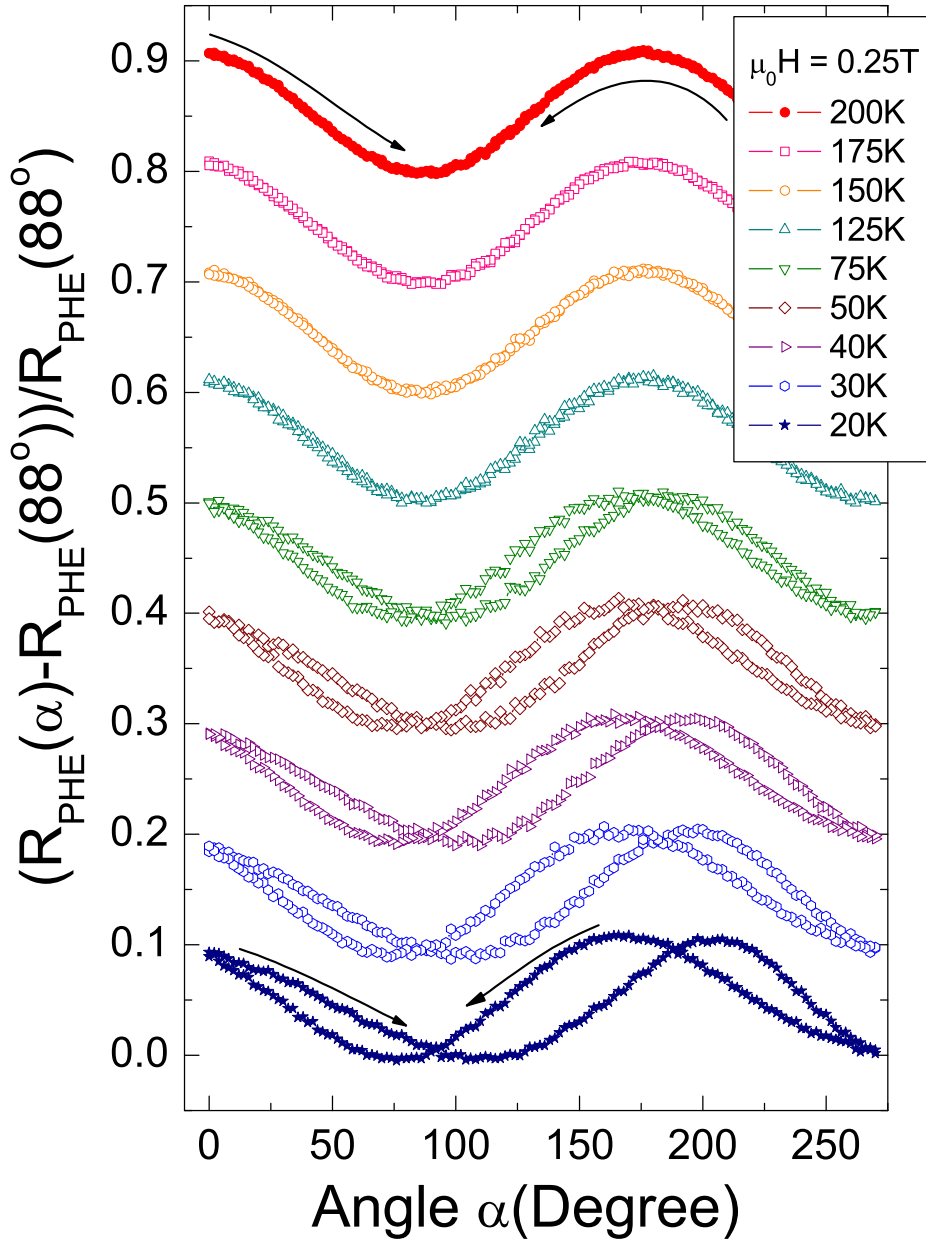


Figure 8. PHE measurements in cycle modus at different constant temperatures and at constant applied field of $\mu_0 H = 0.25$ T. The curves are normalized at their corresponding R_{PHE} values at $\alpha = 88^\circ$. Note that the initial and final values are the same within experimental uncertainty. The measurements were done starting always from the ZFC state at each temperature.

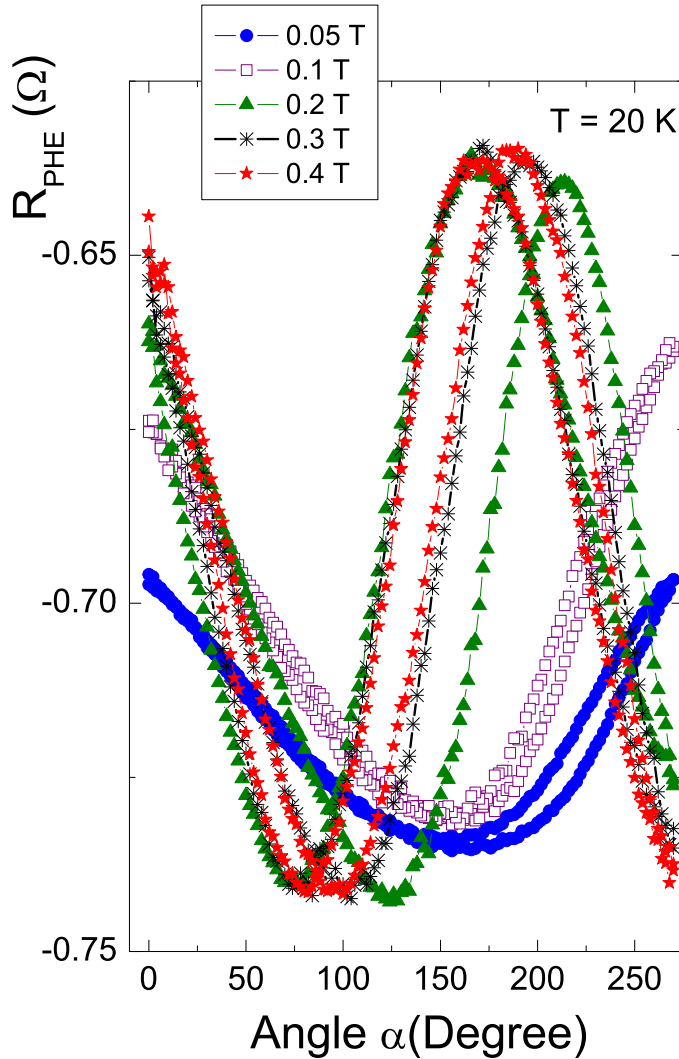


Figure 9. PHE measurements in the ZFC state and at $T = 20$ K at different constant applied fields.

should be directly related to an exchange bias effect. After this experimental observation we have fixed the angle α such that \mathbf{M} was parallel to the main axis of the sample and performed a field dependent measurement of the PHE at FC and ZFC states, see Fig. 11. We found open and close hysteretic loops for the FC and ZFC state, respectively, in good agreement with the results of Fig. 10. For a fixed magnetic field value, see Fig. 11, the PHE resistance increases in the FC state indicating that it is highly sensitive to the exchange bias effects due to pinned magnetic moments or domains at the interface. These results are compatible with a scenario where an interfacial domain structure is present in the ferromagnetic Co layer [35, 45].

These results suggest us to use the transport properties to investigate the exchange-bias effect, as a way to strengthen the interpretation of the magnetization measurements

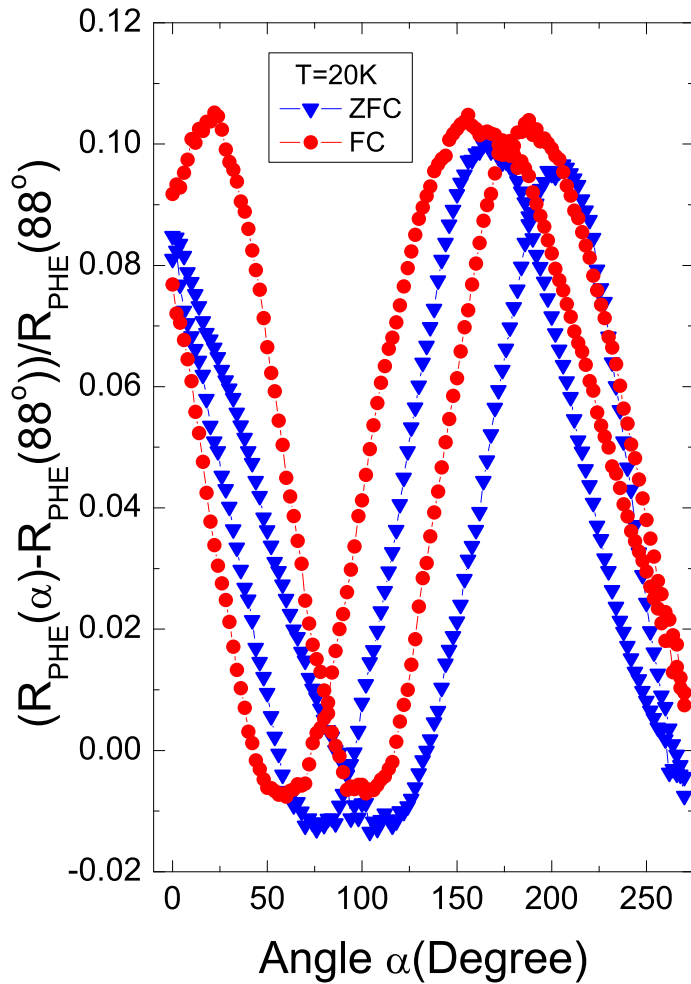


Figure 10. PHE measurements (normalized at their corresponding values for $\alpha = 88^\circ$) as a function of the angle α at a constant applied field $\mu_0 H = 0.25$ T. The measurements were done at $T = 20$ K in a ZFC and FC states.

done with the SQUID. Similar to the SQUID measurements shown in Fig. 3, Fig. 12 shows the MR and PHE measurements at two different temperatures and after cooling the sample with a positive and negative magnetic field of ± 1 T. We observe that after the first reversal process (arrows (1) and (1')) the MR shows a sharp change, while in the second reversal process (arrows (2) and (2')) the change is more rounded and larger in amplitude compared to the first one. This indicates that during the first magnetization reversal there are less moments contributing to the magnetization rotation compared to the subsequent reversal process [45]. The field shifting and asymmetries observed in the MR and PHE are in agreement with the ones observed in the SQUID measurements indicating that the same effects (domain wall propagation and nucleation) contribute in a similar manner in these properties. In both kinds of measurements, we observe that

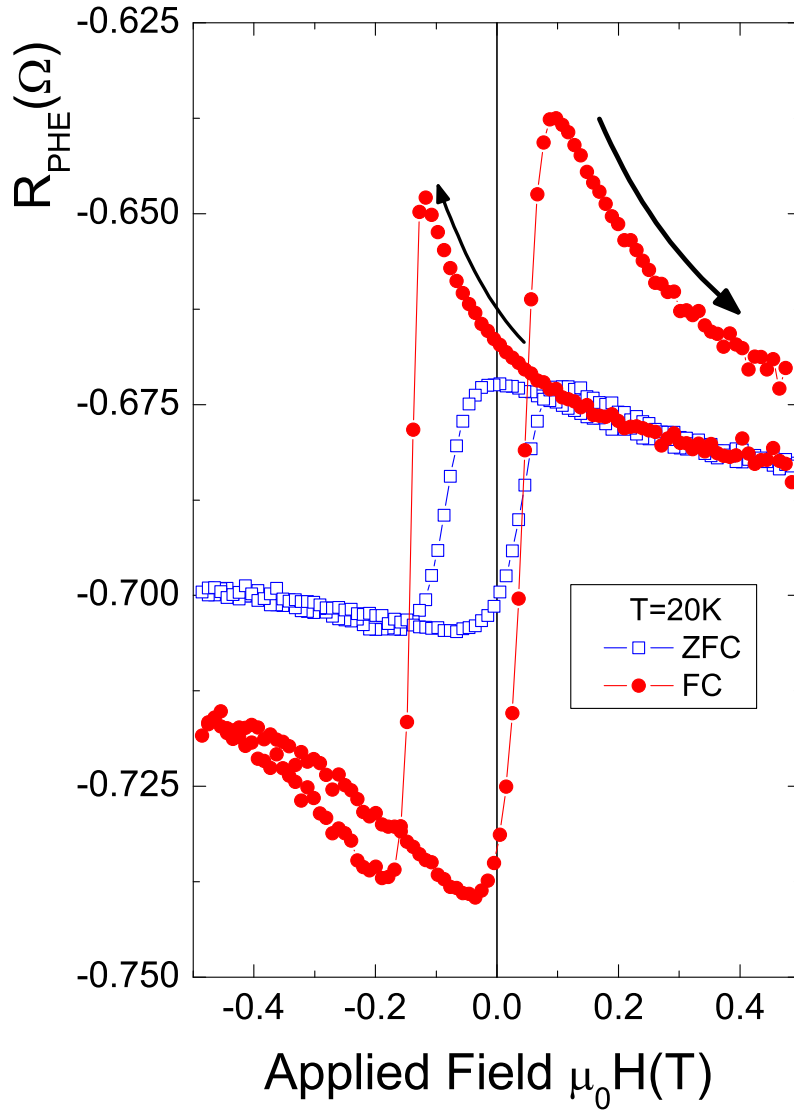


Figure 11. PHE measurement at fixed angle corresponding to the situation where the magnetic field \mathbf{B} and current direction are parallel. The measurements were done at $T = 20$ K in the ZFC and FC ($\mu_0 H_{FC} = 1$ T) states.

at the fields of, e.g. $+0.5$ T or -0.5 T, the initial and final values are not the same, i.e. the MR and PHE show a clear irreversible behavior after completing the field cycle. This irreversibility is more evident in the PHE compared to the AMR results, and both strengthen the existence of the m_{shift} effect measured with the SQUID.

Figure 13 shows the results obtained for the MR and the PHE as a function of applied field at cooling fields $H_{FC} = \pm 1$ T at different constant temperatures. The exchange bias effects are manifested in: - the field and saturation asymmetries, - the different shape at the fields where the magnetization direction changes, and - by the

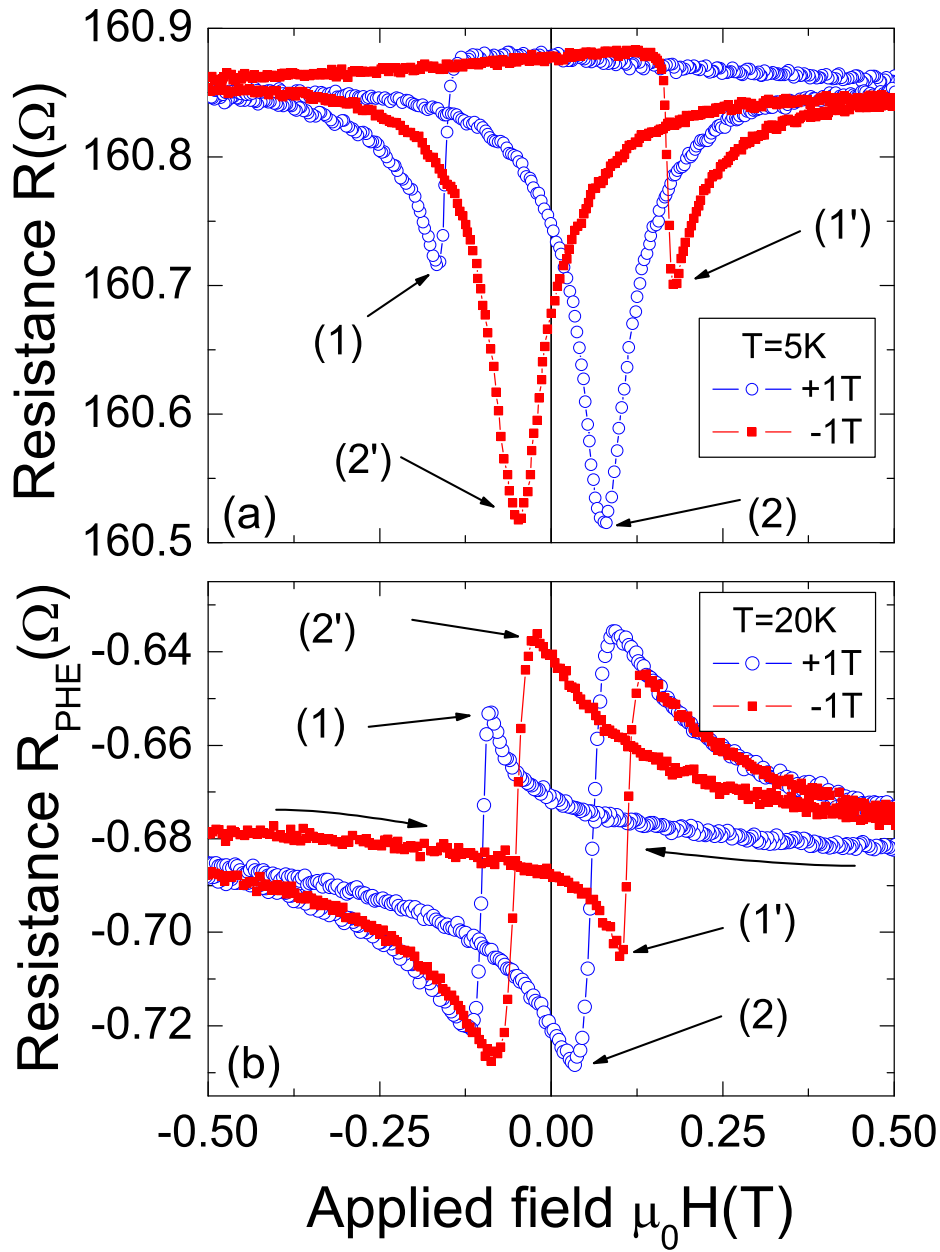


Figure 12. (a) Magnetoresistance and (b) the planar Hall effect measured at 5 K and 20 K, respectively, using positive and negative cooling field $|\mu_0 H_{\text{FC}}| = 1$ T. The numbers in brackets indicate similar features as observed in magnetization measurements in Fig. 3.

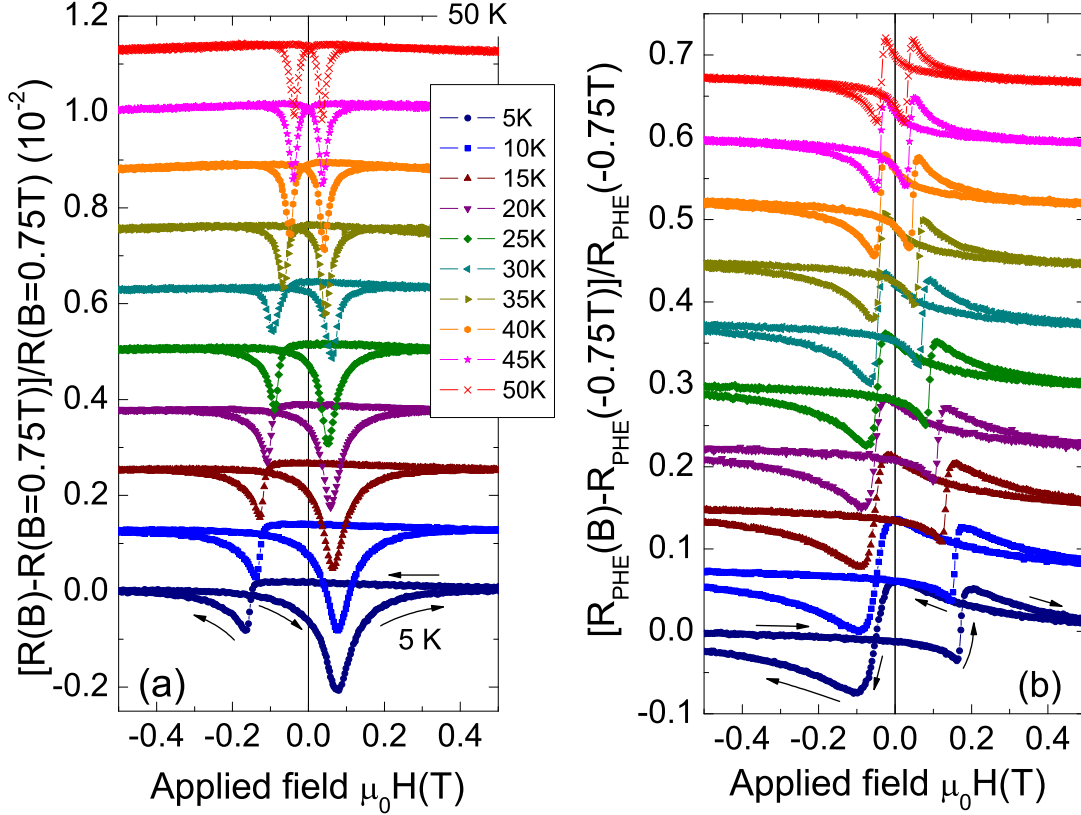


Figure 13. Magnetoresistance (a) and the planar Hall effect (b) measured using a positive and negative cooling field $|\mu_0 H_{FC}| = 1$ T, respectively.

smearing of these characteristics increasing temperature and their vanishing at or just above the Néel temperature. Assuming that the two minima in the MR and the sharp steps in the PHE define the coercive fields, we apply a similar definition as before to estimate the exchange bias field from these two properties H_{E-MR} and H_{E-PHE} . The temperature dependence of these exchange fields are shown in Fig. 14. The nearly linear behavior agrees with that obtained from the SQUID measurements, see Fig. 5. Note that the absolute H_E values obtained from the transport data (Fig. 14) are larger than for the SQUID data (Fig. 5) just because we compare data obtained at different H_{FC} .

The analogous to the magnetic moment shift observed in the SQUID measurement appears also in the MR and PHR measurements, i.e. an irreversibility in the resistance or Hall resistance at the same field after completing a field cycle. As in the case of magnetization measurements, we quantify this irreversibility by the definition, in case of the PHE shift, $R_{PHE-shift} = R_{PHE}(-0.4 \text{ T})_{\uparrow} - R_{PHE}(-0.4 \text{ T})_{\downarrow}$, where $R_{PHE}(-0.4 \text{ T})_{\uparrow}$

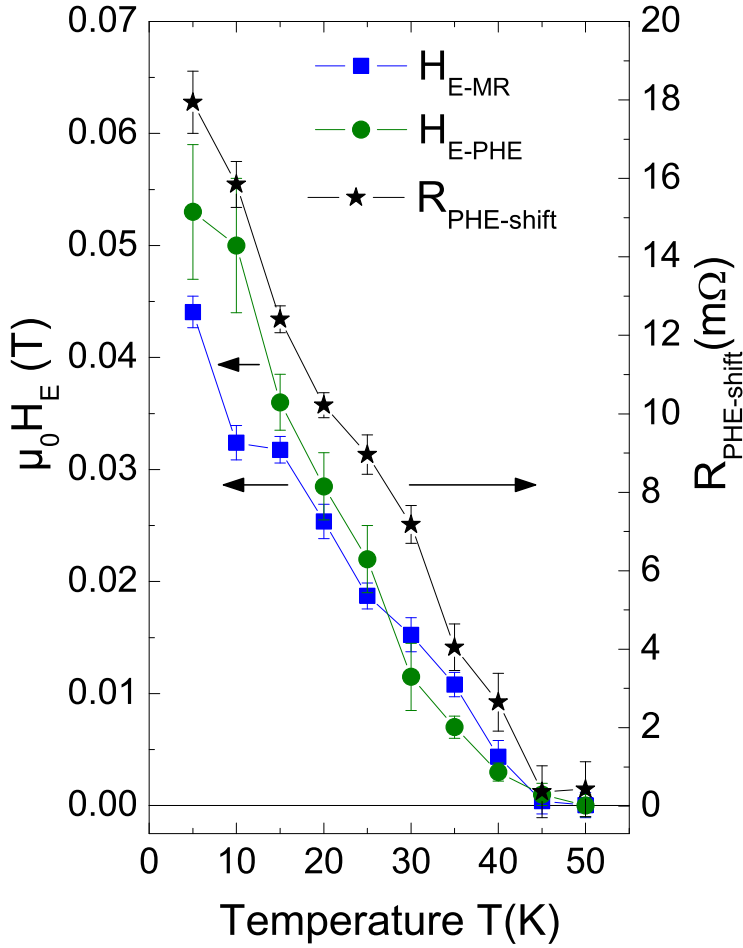


Figure 14. Left y -axis: Exchange bias fields obtained from the magnetoresistance (H_{E-MR}) and from the planar Hall effect (H_{E-PHE}). Right y -axis: Resistance shift in the PHE calculated at $\mu_0 H = -0.4$ T from the data in Fig. 13(b).

means the planar Hall resistance at -0.4 T increasing field from $H_{FC} = -1$ T and $R_H(-0.4 \text{ T}) \downarrow$ the value obtained at the same field but coming from positive fields. Figure 14 shows the obtained temperature dependence of the parameter $R_{PHE-shift}(T)$. From the comparison with $H_E(T)$, it is reasonable to assume that the origin of the exchange bias parameter $R_{PHE-shift}(T)$ is the same as the m_{shift} from SQUID measurements and should be directly correlated with the pinning of domains or magnetic moments of the FM Co layer due to its common interface with the AFM layer. We stress that although the measured transport properties provide information only of the Co layer, it is clear that all exchange bias effects are related to the influence of the AFM layer on the Co layer at the interface.

Note that $R_{PHE-shift}(T)$ does appear to show slight changes of slope at 30 K and 20 K, which may be related to the ferroelectric transition of the o-YMO layer, although

they are not as clear as for the $m_{\text{shift}}(T)$ obtained from the SQUID measurements. This difference between the temperature dependence of these two quantities, $R_{PHE\text{-shift}}(T)$ and $m_{\text{shift}}(T)$, is related to the different H_{FC} used and in part to the field we used to calculate $R_{PHE\text{-shift}}(T)$. Note that the H_{FC} dependence of the m_{shift} is non monotonous, i.e. $M_E \rightarrow 0$ for $H_{FC} \rightarrow \infty$ as well as at $H_{FC} = 0$, as has been shown for La_{0.7}Sr_{0.3}MnO₃/o-YMO bilayers [16].

4. Magneto-transport and SQUID measurements of the Co/CoO wires

The exchange bias effects of the array of 8,500 micro-wires were measured with a SQUID. For the FC measurements the sample was mounted in the SQUID after the corresponding H_{FC} was applied. These measurements reveal shifts in both axis of the hysteresis, similar to that shown in Fig. 3 for the Co/YMO bilayer and we do not need to show them here. Figure 15 shows the temperature dependence of the exchange bias field H_E defined as before and the magnetization shift (M_E -effect) normalized by its value at saturation. The vertical magnetic moment shift m_{shift} is defined as before and at ± 0.1 T. One can clearly recognize in Fig. 15 that both exchange bias effects (red symbols) show a similar temperature dependence.

A typical hysteresis in the magnetoresistance of a single Co/CoO micro-wire is shown in Fig. 16 after cooling the sample in a field of -8 T at two different temperatures. The asymmetry in the coercive field (at the minima) as well as in the saturation region $R_{\text{shift}} = R(-0.1 \text{ T}) - R(+0.1 \text{ T}) > 0$ can be clearly recognized in the figure at 4 K, similarly to the one obtained for the bilayer Co/YMO, see Fig. 12(a). The red curve at 4K shown in the main panel is the hysteresis measured the second time after one cycle to $+0.1 \text{ T} \Rightarrow -0.1 \text{ T}$. In the inset we show the irreversibility in the resistance after the first hysteresis, similar to the irreversibility measured in the Co-YMO bilayer, see Fig. 12(a). The two exchange bias effects obtained from transport measurements of a single micro-wire show similar temperature dependence between each other and to the SQUID results, see Fig. 15. In our samples the exchange bias effects vanish at about 150 K. This may be due to the small thickness of the AF CoO layer. A blocking temperature in this range has been reported for equally thin layers [50]. We think that the results in Co/CoO micro-wires leave little doubt about the existence of both exchange bias effects. Because of the negligible conductance of the oxide layer in comparison with the Co part at the temperature of the measurements, the transport results also indicate that the origin of the magnetization shift comes from the AFM Co layer at the interface with the CoO layer, in agreement with the main results obtained for the Co/YMO bilayer.

5. Conclusion

In the present work we have systematically investigated the exchange bias phenomenon in the novel Co/YMO bilayer using SQUID magnetometry and magneto-transport

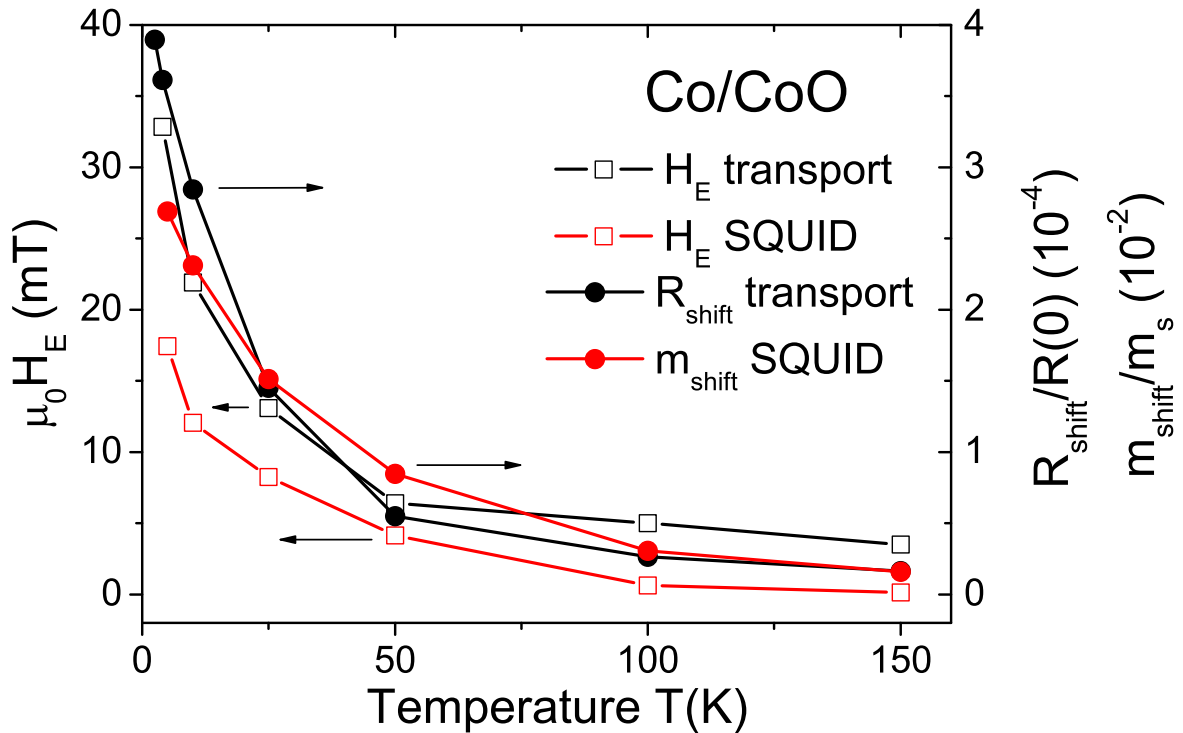


Figure 15. Exchange bias field H_E and normalized magnetic moment shift m_{shift} (right y -axis) measured with a SQUID on an array of 8,500 micro-wires of Co/CoO (red symbols). Similar exchange bias parameters obtained from transport measurements (see Fig. 16) on a single Co/CoO micro-wire.

properties. The extracted exchange bias anomalies show the expected field asymmetry, decreasing nearly linearly with temperature. Additionally, a vertical shift is observed in all measurements, which is related to the pinning of magnetic entities of the ferromagnetic Co layer at the interface with the o-YMO layer. Both exchange bias shifts vanish at or just above the Néel temperature confirming also that these are related to the exchange bias phenomenon. From the magnetization values of Co and o-YMO layers and the observed m_{shift} we can also conclude that the measured M_E effect in the bilayer is a direct contribution from the FM layer. The magneto-transport results provide a clear support to this conclusion. The results obtained from similar magnetization and transport measurements in Co/CoO micro-wires support the main conclusions given above, and stress that the observed phenomena are general and not because of any special magnetic characteristics of the o-YMO layer.

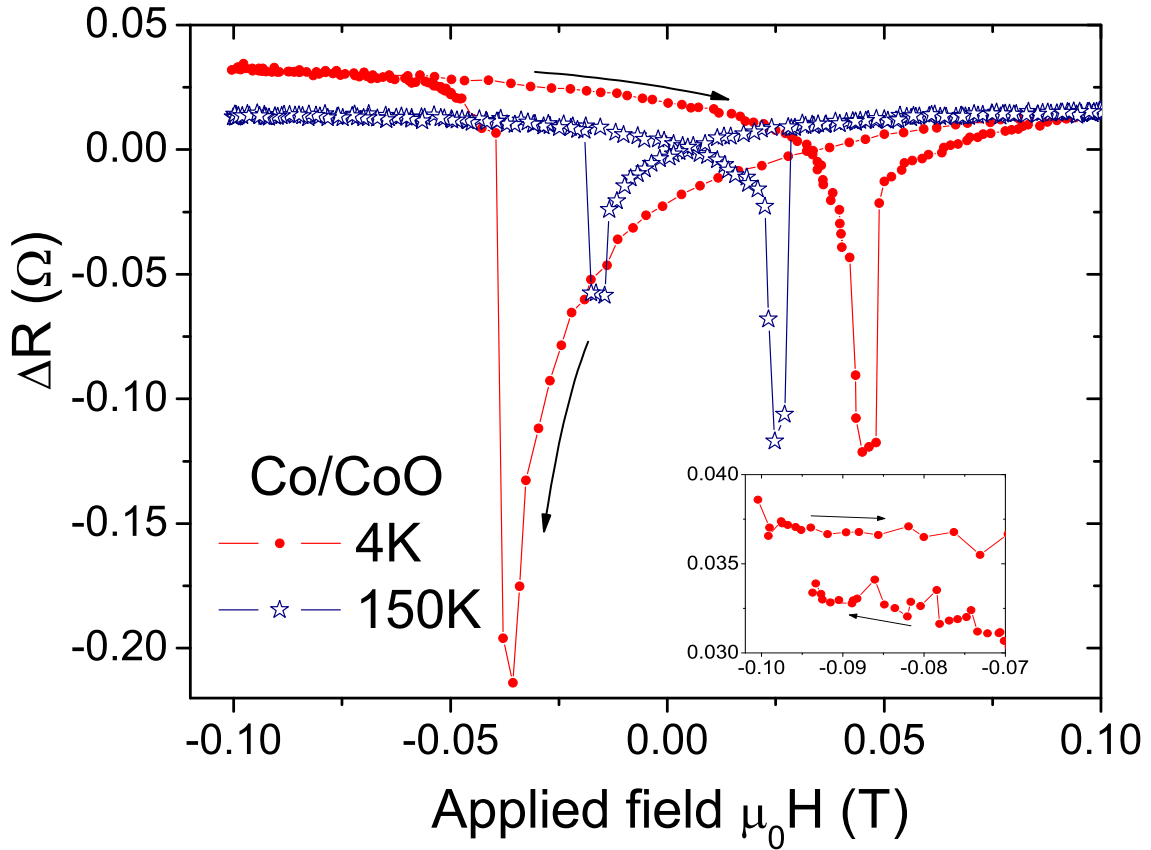


Figure 16. Magnetoresistance defined as $\Delta R = R - R_{\text{intersect}}$ at two temperatures of a single Co/CoO micro-wire. $R_{\text{intersect}}$ is defined as the resistance at which the increasing and decreasing field curves intersect. The sample was measured after cooling in a field of -8 T applied along the principal wire axis. The inset shows the measured curves at the first field cycle near -0.1 T.

Acknowledgments

One of us (C.Z.) was supported by the Sächsisches Staatsministerium für Wissenschaft und Kunst under 4-7531.50-04-0361-09/1. This work was supported by the Collaborative Research Center SFB 762 “Functionality of Oxide Interfaces”

References

- [1] M. Gruyters and D. Riegel. *Phys. Rev. B*, 63:052401, 2000.
- [2] M. H. Francombe and R. W. Hoffman, editors. *Physics of thin films*, volume 6. Academic Press, New York, 1971.
- [3] G. T. Rado and H. Suhl, editors. *Magnetism*. Academic Press, New York, 1963.

- [4] W. H. Meiklejohn and C. P. Bean. *Phys. Rev.*, 102:1413, 1956.
- [5] T. Gredig, I. N. Krivorotov, and E. D. Dahlberg. *Journal of Applied Physics*, 91:7760, 2002.
- [6] D. Tripathy and A. O. Adeyeye. *Phys. Rev. B*, 79:064413, 2009.
- [7] Y. Shimazu, M. Ohkubo, and K. Morinaga. *J. Magn. Magn. Mater.*, 240:17, 2002.
- [8] D. W. Kim, D.-W. Kima, T. W. Noha, H. Tanakac, and T. Kawaic. *Sol. State. Comm.*, 125:305–309, 2003.
- [9] S. Nicolodi, L.G. Pereira, J.E. Schmidt, L.C.C.M. Nagamine, A.D.C. Viegas, C. Deranlot, F. Petroff, and J. Geshev. *Physica B: Condensed Matter*, 384(12):141 – 143, 2006.
- [10] L.C.C.M. Nagamine, J.E. Schmidt, M.N. Baibich, E.B. Saitovitch, and J. Geshev. *Physica B: Condensed Matter*, 384(12):132 – 134, 2006.
- [11] T. R. McGuire and R. I. Plotter. *IEEE Trans. Magn.*, MAG-11:1018, 1975.
- [12] L. Ejsing, M. F. Hansen, A. K. Menon, H. A. Ferreira, D. L. Graham, and P. P. Freitas. *Appl. Phys. Lett.*, 84:4729, 2004.
- [13] C. D. Damsgaard, S. C. Freitas, P. P. Freitas, and M. F. Hansen. *Journal of Applied Physics*, 103:07A302, 2008.
- [14] A. D. Henriksen, B. T. Dalslet, D. H. Skieller, K. H. Lee, F. Okkels, and M. F. Hansen. *Appl. Phys. Lett.*, 97:013507, 2010.
- [15] H. Y. Hwang, Y. Iwasa, M. Kawasaki, B. Keimer, N. Nagaosa, and Y. Tokura. *Nature Materials*, 11:103–113, 2012.
- [16] C. Zandalazini, P. Esquinazi, G. Bridoux, J. Barzola-Quiquia, H. Ohldag, and E. Arenholz. *J. Magn. Magn. Mater.*, 323:2892–2898, 2011.
- [17] J. de la Venta, M. Erekhinsky, Siming Wang, K. G. West, R. Morales, and Ivan K. Schuller. *Phys. Rev. B*, 85:134447, Apr 2012.
- [18] M. R. Fitzsimmons, B. J. Kirby, S. Roy, Zhi-Pan Li, Igor V. Roshchin, S. K. Sinha, and I. V. Schuller. *Phys. Rev. B*, 75:214412, 2007.
- [19] Hendrik Ohldag, Hongtao Shi, Elke Arenholz, Joachim Stöhr, and David Lederman. *Phys. Rev. Lett.*, 96:027203, 2006.
- [20] R. Morales, Z.-P. Li, O. Petravic, X. Battle, I. K. Schuller, J. Olamit, and K.. Liu. *Appl. Phys. Lett.*, 89:072504, 2006.
- [21] I. Campbell and A. Fert. *Ferromagnetic Materials*, volume 3, page 762. North-Holland Publishing Company, Amsterdam, 1982.
- [22] H.L. Yakel, W. D. Koehler, E. F. Bertaut, and F. Forrat. *Acta Crystallogr.*, 16:957, 1963.
- [23] A. Waintal and J. Chenavas. *Compt. Rend.*, 264:B 168, 1967. see also *Mat. Res. Bull.* **2**, 819 (1967).
- [24] V. E. Wood, A.E. Austin, and E. W. Collings. *J. Phys. Chem. Solids*, 34:859, 1973.
- [25] O. Yu Gorbenko, S. V. Samoilenkov, I. E. Graboy, and A. R. Kaul. *Chem. Mater.*, 14:4026, 2002.
- [26] X. Martí, F. Sánchez, V. Skumryev, V. Laukhin, C. Ferrater, M. V. García-Cuenca, M. Varela, and J. Fontcuberta. *Thin Sol. Films*, 516:4899–4907, 2008.
- [27] P. A. Salvador, T. D. Doan, B. Mercey, and B. Raveau. *Chem. Mater.*, 10:2592, 1998.
- [28] X. Martí, F. Sánchez, J. Fontcuberta, M.V. García-Cuenca, C. Ferrater, and M. Varela. *Journal of Applied Physics*, 99:08P302, 2006.
- [29] C. C. Hsieh, T. H. Lin, H. C. Shih, C.-H. Hsu, C. W. Luo, J.-Y. Lin, K. H. Wu, T. M. Uen, and J. Y. Juang. *Journal of Applied Physics*, 104:103912, 2008.
- [30] J. Kim, S. Jung, M. S. Park, Sung-Ik Lee, H. D. Drew, H. Cheong, K. H. Kim, and E. J. Choi. *Phys. Rev. B*, 74:052406, 2006.
- [31] F. Demmel and T. Chatterji. *Phys. Rev. B*, 76:212402, 2007.
- [32] P. Miltényi, M. Gierlings, J. Keller, B. Beschoten, G. Güntherodt, U. Nowak, and K. D. Usadel. *Phys. Rev. Lett.*, 84:4224, 2000.
- [33] J. Keller, P. Miltényi, B. Beschoten, G. Güntherodt, U. Nowak, and K. D. Usadel. *Phys. Rev. B*, 66:014431, 2002.
- [34] U. Nowak, A. Misra, and K. D. Usadel. *J. Magn. Magn. Mat.*, 240:243–247, 2002.

- [35] F. Radu, M. Etzkorn, R. Siebrecht, T. Schmitte, K. Westerholt, and H. Zabel. *Phys. Rev. B*, 67:134409, 2003.
- [36] F. Radu and H. Zabel. *Magnetic Heterostructures*, volume 227 of *STMP*. H. Zabel and S. D. Bader (eds.), Springer Berlin, Heidelberg, 2008.
- [37] A. Muñoz, J. A. Alonso, M. T. Casais, M. J. Martinez-Lopez, J. L. Martinez, and M. T. Fernandez-Diaz. *J. Phys.: Condens. Matter*, 14:3285–3294, 2002.
- [38] J. Nogués and I. K. Schuller. *J. Magn. Magn. Mat.*, 192:203–232, 1999.
- [39] J. Nogués, D. Lederman, T. J. Moran, and I. K. Schuller. *Phys. Rev. Lett.*, 76:4624, 1996.
- [40] M. Kiwi, J. Mejía-López, R. D. Portugal, and R. Ramirez. *Solid State Commun.*, 166:315–319, 2000.
- [41] C. Nogués, C. Leighton, and I. K. Schuller. *Phys. Rev. B*, 61:1315, 2000.
- [42] Julio Camarero, Jordi Sort, Axel Hoffmann, Jose Miguel García-Martín, Bernard Dieny, Rodolfo Miranda, and Josep Nogués. *Phys. Rev. Lett.*, 95:057204, 2005.
- [43] M. Gierlings, M. J. Prandolini, H. Fritzsche, M. Gruyters, and D. Riegel. *Phys. Rev. B*, 65:092407, 2002.
- [44] A. Hoffmann. *Phys. Rev. Lett.*, 63:097203, 2004.
- [45] S. Brems, D. Buntinx, K. Temst, and C. Van Haesendonck. *Phys. Rev. Lett.*, 95:157202, 2005.
- [46] J. Barzola-Quiquia, P. Esquinazi, M. Rothermel, D. Spemann, A. Setzer, and T. Butz. *Nucl. Instrum. Methods Phys. Res. B*, 256:412–418, 2007.
- [47] A. P. Malozemoff. *Journal of Applied Physics*, 63:3874, 1988.
- [48] A. L. Efros and B. I. Shklovskii. *Journal of Physics C: Solid State Physics*, 8:L49, 1975.
- [49] W. Gil, D. Görlitz, M. Horisberger, and J. Kötzler. *Phys. Rev. B*, 72:134401, 2005.
- [50] D. Buntinx, S. Brems, A. Volodin, K. Temst, and C. Van Haesendonck. *Phys. Rev. Lett.*, 94:017204, 2005.